Langmuir
Article
pubs.acs.org/Langmuir

Stress Buildup under Start-Up Shear Flows in Self-Assembled Transient Networks of Telechelic Associating Polymers†

Tsuyoshi Koga,‡ Fumihiko Tanaka,*,‡ Isamu Kaneda,§ and Françoise M. Winnik∥

‡Department of Polymer Chemistry, Graduate School of Engineering, Kyoto University, Katsura, Kyoto 615-8510, Japan, §Department of Food Science, Rakuno Gakuen University, Ebetsu, Hokkaido 069-8501, Japan, and ∥Department of Chemistry and Faculty of Pharmacy, University of Montréal, CP 6128, Succursale Centre Ville, Montréal QC, Canada H3C 3J7

Received December 23, 2008. Revised Manuscript Received February 17, 2009

The nonaffine transient network theory is used to study the time development of the shear and normal stresses under start-up shear flows in networks formed by self-assembled telechelic, hydrophobically modified water-soluble polymers. The initial slope, strain hardening, and overshoot of the shear stress are studied in detail in relation to the nonlinear tension−elongation curve of the elastically active chains in the network. The condition for the occurrence of strain hardening (upward deviation of the stress from the reference curve defined by the linear moduli) is found to be $\dot{\gamma} > \dot{\gamma}_c(A)$, where $\dot{\gamma}$ is the shear rate, $\dot{\gamma}_c$ is its critical value for strain hardening, and A is the amplitude of the nonlinear term in the tension of a chain. The critical shear rate $\dot{\gamma}_c$ is calculated as a function of A. It is approximately 6.3 (in the time unit of the reciprocal thermal dissociation rate) for a nonlinear chain with $A = 10$. The overshoot time t_{max} when the stress reaches a maximum and the total deformation $\gamma_{max} \equiv \dot{\gamma} t_{max}$ accumulated before the peak time are obtained in terms of the molecular parameters of the polymer chain. The maximum deformation γ_{max} turns out to depend weakly upon the shear rate $\dot{\gamma}$. The first and second normal stress differences are also studied on the basis of the exact numerical integration of the theoretical model by paying special attention to their overshoot, undershoot, and sign change as a function of the shear rate. These theoretical results are compared with recent rheological experiments of the solutions of telechelic hydrophobically modified poly(ethylene oxide)s carrying short branched alkyl chains (2-decyl-tetradecyl) at both ends.

1. Introduction

The rheological properties of the transient networks formed by associating polymers have attracted much experimental and theoretical interest in recent years. Typical examples of these systems are networks created in aqueous solutions of hydrophilic polymers with short hydrophobic chains attached at both chain ends (telechelic polymers), such as hydrophobic ethoxylated urethane (called HEUR),[1−4] hydrophobic poly(*N*-isopropylacrylamide),[5,6] and poly(propylene oxide)-poly(ethylene oxide)-poly(propylene oxide) triblock copolymers.[7−9]

A simple theory of the transient networks in which network junctions can break and recombine by thermal motion of the polymers and/or under applied deformation was proposed by Green and Tobolsky[10] and later developed by Lodge[11] and Yamamoto.[12] More recently, one of us and Edwards[13,14] (referred to as TE) refined their theory for networks made up of telechelic associating polymers in order to establish a detailed molecular−theoretical picture for the Maxwellian behavior of the dynamic mechanical moduli and also to account for the observed shear-rate dependence of the nonlinear viscosity. The fundamental assumption of TE theory is the affine deformation of the network junctions as in the classical theory of rubber elasticity; the end-to-end vector of a bridge chain connecting the neighboring micellar junctions deforms affinely to the macroscopic deformation tensor.[15,16] We have recently developed a new nonaffine transient network theory[17] (referred to as TK) in which the affiness assumption is entirely eliminated. The network junctions are allowed to fluctuate in space and to diffuse from their average positions that move affinely to the macroscopic flow fields. TK is the counterpart of the phantom network theory of rubber elasticity with permanent junctions, developed by James and Guth,[18,19] extended to the networks with temporal junctions. It can study the long-time diffusion (tracer diffusion) of a marked chain by the repetition of association−dissociation processes of either chain end without complete separation from the network (looper mode).

Consider, as in TE, a bridge chain connecting two junctions in the network. If the average diffusion constant of the network junctions is well-defined and given by D, then the mean square radius $\langle(\Delta r)^2\rangle$ of the displacement made by a junction to which the

† Part of the Molecular and Polymer Gels; Materials with Self-Assembled Fibrillar Networks special issue.

*Corresponding author. E-mail: ftanaka@phys.polym.kyoto-u.ac.jp.

(1) Jenkins, R. D.; Silebi, C. A.; El-Asser, M. S. In *Polymers as Rheology Modifiers*; ACS Symposium Series 462; Schulz, D. N., Glass, J. E., Eds.; American Chemical Society: Washington, DC, 1991; p 222.
(2) Annable, T.; Buscall, R.; Ettelaie, R.; Whittlestone, D. *J. Rheol.* **1993**, *37*, 695.
(3) Annable, T.; Buscall, R.; Ettelaie, R.; Shepherd, P.; Whittlestone, D. *Langmuir* **1994**, *10*, 1060.
(4) Yekta, A.; Xu, B.; Duhamel, J.; Adiwidjaja, H.; Winnik, M. A. *Macromolecules* **1995**, *28*, 956.
(5) Kujawa, P.; Watanabe, H.; Tanaka, F.; Winnik, F. M. *Eur. Phys. J. E* **2005**, *17*, 129.
(6) Kujawa, P.; Segui, F.; Shaban, S.; Diab, C.; Okada, Y.; Tanaka, F.; Winnik, F. M. *Macromolecules* **2006**, *39*, 341.
(7) Quellet, C.; Eicke, H.-F.; Xu, G.; Hauger, Y. *Macromolecules* **1990**, *23*, 3347.
(8) Mortensen, K.; Brown, W.; Norden, B. *Phys. Rev. Lett.* **1992**, *68*, 2340.
(9) Odenwald, M.; Eicke, H.-F.; Meier, W. *Macromolecules* **1995**, *28*, 5069.
(10) Green, M. S.; Tobolsky, A. V. *J. Chem. Phys.* **1946**, *14*, 80.
(11) Lodge, A. S. *Trans. Faraday Soc.* **1956**, *52*, 120.
(12) Yamamoto, M. *J. Phys. Soc. Jpn.* **1956**, *11*, 413; **1957**, *12*, 1148; **1958**, *13*, 1200.
(13) Tanaka, F.; Edwards, S. F. *Macromolecules* **1992**, *25*, 1516.
(14) Tanaka, F.; Edwards, S. F. *J. Non-Newtonian Fluid Mech.* **1992**, *43*, 247, 272, 289.
(15) Kuhn, W. *J. Polym. Sci.* **1946**, *1*, 380.
(16) Flory, P. J. *Principles of Polymer Chemistry*; Cornell University Press: New York, 1953; Chapter XI.
(17) Tanaka, F.; Koga, T. *Macromolecules* **2006**, *39*, 5913.
(18) James, H. M. *J. Chem. Phys.* **1947**, *15*, 651.
(19) James, H. M.; Guth, E. *J. Chem. Phys.* **1947**, *15*, 669.

bridge chain is attached before its end is dissociated is given by $D\beta_0^{-1}$, where β_0 is the thermal dissociation rate. In TK, we introduced a fundamental dynamic parameter, the ratio of the diffusion radius to the mean square end-to-end distance $\langle r^2\rangle_0 = na^2$ of the bridge chain

$$\epsilon_D \equiv D\beta_0{}^{-1}/na^2 \tag{1.1}$$

where n is the number of statistical units on a chain and a is the size of the statistical repeat unit. If ϵ_D is small, then the network is well described by the affine network of TE, but if ϵ_D is on the order of unity, then the effect of fluctuations is large so that the effect of diffusion must be examined by TK. TK showed that the profile of the calculated dynamic mechanical moduli deviates from that of a Maxwell fluid with a single relaxation time. The storage modulus is softened at low frequencies, whereas the loss modulus loses its symmetric profile by forming a high-frequency tail.

As for the nonlinear stationary viscosity, Indei et al.[20] found the necessary condition for the appearance of shear-thickening phenomena in terms of the molecular properties of the constituent polymer chains and constructed a thickening−thinning phase diagram.

The main purpose of this article is to study the transient flows in solutions of telechelic associating polymers beyond the linear regime. We specifically study the shear flows that are started at a certain time in the network in equilibrium with a constant shear rate (start-up shear flow). We calculate the growth function of the shear and normal stresses mostly within the theoretical framework of TE but also by TK whenever calculation is possible. In particular, we find the conditions for the occurrence of strain hardening and stress overshoot in terms of the molecular parameters.

2. Nonaffine Transient Network Theory

Consider transient networks made up of telechelic polymers carrying short hydrophobic groups at their chain ends (Figure 1). In the network of telechelic polymers, there are two kinds of polymer chains: elastically effective chains that bridge the different micellar junctions and dangling chains with one end dissociated from the junction and free to move. We neglect loop chains dangling from the junctions because they reduce only the absolute values of moduli. The total length of the chain is given by $l \equiv na$. (We neglect the length of the end chains by assuming that they are negligibly short compared with the middle chain.) Typical polymers used in the experiments are poly(ethylene oxide) (PEO) of molecular weight ranging from 6×10^3 to 35×10^3 g mol^{-1} carrying alkyl chains $-C_kH_{2k+1}$ with k ranging from 12 to 22,[1−4] poly(*N*-isopropylacrylamide) (PNIPAM) of molecular weight ranging from 7×10^3 to 5.9×10^4 g mol^{-1} with $k = 18$.[5,6]

Suppose the network is subjected to a time-dependent deformation described by the tensor $\hat{\lambda}(t)$. It can be a shear flow or an elongational flow and does not need to be specified at this stage. Let ν be the number of chains in a unit volume, let $\psi(\mathbf{r}, t)$ be the number of bridge chains per unit volume at time t whose end-to-end vector is given by $\mathbf{r}$, and let $\phi(\mathbf{r}, t)$ be the number of dangling chains (Figure 1). Let $\mathbf{f}(\mathbf{r})$ be the tension along the bridge chain as a function of vector $\mathbf{r}$. Then, TK found that ψ and ϕ satisfy the coupled equations

$$\frac{\partial}{\partial t}\psi(\mathbf{r},t) + \nabla\cdot(\bar{\mathbf{v}}(t)\,\psi(\mathbf{r},t)) = D\nabla\cdot[\nabla + \mathbf{f}/k_BT + \nabla \ln K(\mathbf{r})]\psi(\mathbf{r},t) - \beta(\mathbf{r})\,\psi(\mathbf{r},t) + \alpha(\mathbf{r})\,\phi(\mathbf{r},t), \tag{2.1a}$$

$$\frac{\partial}{\partial t}\phi(\mathbf{r},t) = D_1\nabla\cdot[\nabla + \mathbf{f}/k_BT]\phi(\mathbf{r},t) + \beta(\mathbf{r})\,\psi(\mathbf{r},t) - \alpha(\mathbf{r})\,\phi(\mathbf{r},t) \tag{2.1b}$$

(20) Indei, T.; Koga, T.; Tanaka, F. *Macromol. Rapid Commun.* **2005**, *26*, 701.

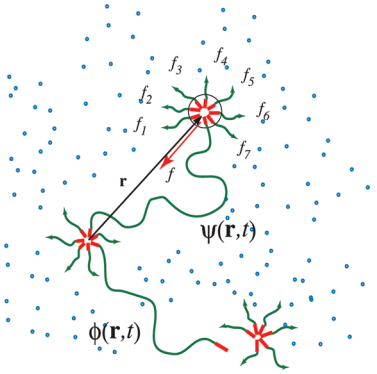

Figure 1. Bridge chain with the end-to-end vector $\mathbf{r}$ and a dangling chain with one free end in the transient network made up of telechelic polymers. Micellar junctions make Brownian motion by the thermal force under tensions $\mathbf{f}_j$ given by the polymer chains whose ends are connected to them. The diffusion constant D of a junction depends upon its aggregation number. The instantaneous vector $\mathbf{r}$ does not change affinely to the external deformation tensor.

where $\alpha(\mathbf{r})$ is the recombination rate (the probability per unit time for a dangling end with end-to-end vector $\mathbf{r}$ to associate to a junction), $\beta(\mathbf{r})$ is the dissociation rate (the probability per unit time for either end of a bridge chain with end-to-end vector $\mathbf{r}$ to dissociate), and $K(\mathbf{r})$ is the equilibrium constant for the reversible dissociation−association reaction. The diffusion constants are given by $D = k_BT/\zeta$ for a micellar junction and $D_1 = k_BT/\zeta_1$ for a free end of the dangling chain, where ζ and ζ_1 are the friction coefficient of the micelle and the end chain. The characteristic time for diffusion is given by $\tau = l^2/D$ for the junctions and $\tau_1 = l^2/D_1$ for the free end of the dangling chains.

The tension along the chain depends upon the nature of the polymer chain. If it is Gaussian, then the relation $\mathbf{f}/k_BT = 3\mathbf{r}/na^2$ holds, and hence the equilibrium distribution function of the end-to-end vector is given by

$$\Phi(\mathbf{r}) = C_n \exp(-3r^2/2na^2) \equiv \Phi_0(\mathbf{r}) \tag{2.2}$$

where the normalization constant is given by $C_n \equiv (3/2\pi na^2)^{3/2}$ under the condition that the upper limit of the integral is allowed to extend to infinity. If it is, for instance, a Langevin chain, then we have

$$fa/k_BT = L^{-1}(r/na) \tag{2.3}$$

and

$$\Phi(\mathbf{r}) = C_n \exp\left[-\int_0^r L^{-1}(r/na)\,\mathrm{d}r/a\right] \tag{2.4}$$

where $L(x) \equiv \coth x - 1/x$ is a Langevin function.[15]

For numerical calculation, we first scale all lengths by using the chain contour length $l = na$ as a unit. We then specify the dimensionless tension $\tilde{f}(\tilde{r}) \equiv f(r)a/k_BT$ as a function of the scaled end-to-end distance $\tilde{r} \equiv r/l$. Let us assume, as in Indei et al.,[20] the simple form

$$\tilde{f}(\tilde{r}) = 3\tilde{r}\left(1 + \frac{2}{3}A\frac{\tilde{r}^2}{1-\tilde{r}^2}\right) \tag{2.5}$$

for the profile (Figure 2). The numerical amplitude A shows the effect of nonlinearity of the chain. If $A = 0$, then the chain reduces to a Gaussian. If $A = 1$, then it agrees with that of a Langevin

chain within a very high accuracy (95%). The nonlinearity increases with amplitude A. Thus, by simply changing A, we can study the effect of a nonlinear elongation of the bridge chains on the rheological properties of the networks.

As for the dissociation rate of the chain ends, it must be an even function of the tension by symmetry. We propose the form

$$\beta(r) = \beta_0(T)[1 + g\tilde{f}(\tilde{r})^2] \tag{2.6}$$

where $\beta_0(T)$ is the thermal dissociation rate and g is the coupling constant between the dissociation rate and the chain tension.[20] This form can be derived by applying the conventional Kramers method[21] to calculate the first passage of time required for a trapped Brownian particle to overcome the barrier height of the force potential. The coupling constant g provides a measure of how easily the end chains are extruded from the micelles to which they are attached. In work by Green and Tobolsky,[10] the dissociation rate was assumed to be independent of the end-to-end vector and hence the chain tension. We therefore go back to their theory by fixing $g = 0$ (referred to as the GT limit). The thermal dissociation rate β_0 depends only on the temperature. In what follows, we use β_0^{-1} as a unit of time so that we may replace $\beta(r) = 1 + g\tilde{f}(\tilde{r})^2$ in all of the integrals given below. The characteristic dimensionless time for diffusion turns out to be $\tau = l^2/D\beta_0^{-1}$ for the junctions and $\tau_1 = l^2/D_1\beta_0^{-1}$ for the end chains.

Let us first find the solution of the coupled equations for ψ and ϕ under no deformation. Network junctions fluctuate around their average positions so that the mean velocity is zero ($\overline{\mathbf{v}}(t) = 0$). Because we have the situation of $D_1 \gg D$, the relaxation time of the free ends is much shorter than that of the micelles. We therefore assume, as in TE, that all of the dangling chains instantaneously relax to their equilibrium conformation and should fulfill the condition

$$(\nabla + \mathbf{f}/k_BT)\phi_0(\mathbf{r}, t) = \mathbf{0} \tag{2.7}$$

Hence, we find that their distribution function is given by

$$\phi_0(\mathbf{r}, t) = \nu_d(t)\,\Phi(\mathbf{r}) \tag{2.8}$$

where $\nu_d(t)$ is the number of dangling chains in a unit volume of the network at time t, and

$$\Phi(\mathbf{r}) \equiv C_n \exp\left[-\int_0^{\mathbf{r}} (\mathbf{f}/k_BT)\cdot d\mathbf{r}\right] \tag{2.9}$$

with C_n being the normalization constant, is the distribution function of the end-to-end vector. Such an assumption of complete relaxation for the dangling chains has recently been examined theoretically[22−24] and experimentally.[25] It was found that, under a certain condition, a high-frequency tail appears in the loss modulus as a result of the incomplete relaxation of the dangling chains within the time interval between their dissociation and recombination. In the present study, we assume the separability of time scales τ_1 and τ due to the large size of the micellar junctions and neglect the effect of incomplete relaxation.

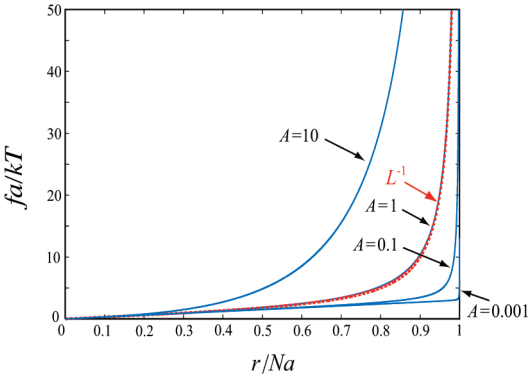

Figure 2. Tension−elongation profile of the model chain used in the transient network theory. It is Gaussian for small elongation but reveals a nonlinear stretching effect characterized by parameter A (nonlinear amplitude). For $A = 1$, the chain reduces to the Langevin chain with high accuracy.

Substituting eq 2.8 into eq 2.1b and integrating the result over all possible values of $\mathbf{r}$, we find

$$d\nu_d(t)/dt = -\langle\alpha\rangle_0\nu_d(t) + \int \beta(\mathbf{r})\,\psi(\mathbf{r}, t)\,d\mathbf{r} \tag{2.10}$$

where

$$\langle\alpha\rangle_0 \equiv \int \alpha(\mathbf{r})\Phi(\mathbf{r})\,d\mathbf{r} \tag{2.11}$$

is the average recombination rate of the free ends. The total number $\nu_e(t)$ of effective chains in a unit volume at time t is then given by

$$\nu_e(t) = \nu - \nu_d(t) \tag{2.12}$$

as a result of the chain conservation law.

Consider next an aged system that has been kept quiescent for a long time so that all chains relax to the equilibrium state. We have $\phi_0(\mathbf{r}) = \nu_d(\infty)\,\Phi(\mathbf{r})$, and from eq 2.1b, we find that the equilibrium distribution of the effective chains takes the form

$$\psi_0(\mathbf{r}) = \nu_d(\infty)\,\alpha(\mathbf{r})\,\Phi(\mathbf{r})/\beta(\mathbf{r}) \tag{2.13}$$

Because the ratio $\beta(\mathbf{r})/\alpha(\mathbf{r})$ is the equilibrium constant $K(\mathbf{r})$ of the chemical reaction between the effective and dangling state, the above equation is transformed to

$$\psi_0(\mathbf{r}) = \nu_d(\infty)C_n \exp\left[-\int_0^{\mathbf{r}} (\mathbf{f}/k_BT + \nabla \ln K(\mathbf{r}))\cdot d\mathbf{r}\right] \tag{2.14}$$

Here, we can explicitly see that an effective chain experiences, in addition to direct tension $\mathbf{f}$ along its contour, the chemical affinity $\nabla \ln K(\mathbf{r})$ caused by the tensions from other chains connected to the same junction. Thus, the total force working on the end of an effective chain is given by

$$\mathbf{F}(\mathbf{r}) \equiv \mathbf{f}/k_BT + \nabla \ln K(\mathbf{r}) \tag{2.15}$$

3. Initial Value Problems

We now specifically study shear flow along the x axis, which starts at time $t = 0$ with a constant shear rate $\dot{\gamma}$ in the transient

(21) Kramers, H. A. *Physica* **1940**, *VII*, 284.
(22) Wang, S.-Q. *Macromolecules* **1992**, *25*, 7003.
(23) Marrucci, G.; Bhargava, S.; Cooper, S. L. *Macromolecules* **1993**, *26*, 6483.
(24) Vaccaro, A.; Marrucci, G. *J. Non-Newtonian Fluid Mech.* **2000**, *121*, 261.
(25) Pellens, L.; Ahn, K. H.; Lee, S. J.; Mewis, J. *J. Non-Newtonian Fluid Mech.* **2004**, *121*, 87.

network of telechelic associating polymers. The average velocity field is given by $\bar{\mathbf{v}}(t) = (\dot{\gamma}y, 0, 0)$, where y is the coordinate axis perpendicular to the flow direction x. We assume that the relaxation time of the dangling chains is sufficiently short compared to that of the active chains so that their distribution function is given by eq 2.8. The equation for the time development of the active chains then takes the form

$$\frac{\partial \psi}{\partial t} + \dot{\gamma} y \frac{\partial \psi}{\partial x} = [D\nabla\cdot(\nabla + \mathbf{F}) - \beta(\mathbf{r})]\psi + \nu_{\mathrm{d}}(t)\, \alpha(\mathbf{r})\, \Phi(\mathbf{r}) \quad (3.1)$$

To solve this equation, we introduce a function $\xi(\mathbf{r},t)$ by the definition $\psi(\mathbf{r},t) \equiv \psi_0(\mathbf{r})\ \xi(\mathbf{r},t)$. It gives the deviation from the equilibrium distribution. Substituting into the above equation and dividing by $\psi_0(\mathbf{r})$, we find the equation for $\xi(\mathbf{r},t)$ to be

$$\frac{\partial \xi}{\partial t} + \dot{\gamma} y \left(\frac{\partial}{\partial x} - \frac{x}{r} F\right)\xi = (D\hat{Q} - \beta(\mathbf{r}))\xi + \beta(\mathbf{r})\zeta(t) \quad (3.2)$$

where the operator $\hat{Q}$ is defined by

$$\hat{Q} \equiv (\nabla - \mathbf{F})\cdot\nabla \quad (3.3)$$

and

$$\zeta(t) \equiv \nu_{\mathrm{d}}(t)/\nu_{\mathrm{d}}(t = 0) \quad (3.4)$$

is the number of dangling chains at time t counted relative to its initial equilibrium value $\nu_{\mathrm{d}}(t = 0)$ without shear. The initial value $\nu_{\mathrm{d}}(t = 0)$ is equivalent to $\nu_{\mathrm{d}}(\infty)$ in eq 2.13.

Our starting equation is then written in compact form as

$$\frac{\partial \xi}{\partial t} + [\dot{\gamma}\hat{P} + \beta(\mathbf{r}) - D\hat{Q}]\xi = \beta(\mathbf{r})\ \zeta(t) \quad (3.5)$$

where the operator $\hat{P}$ is defined by

$$\hat{P} \equiv y\left[\frac{\partial}{\partial x} - \frac{x}{r}F(r)\right] \quad (3.6)$$

The formal solution of this equation with the initial condition $\xi(\mathbf{r}, 0) = 1$ can be written as

$$\xi(\mathbf{r}, t) = \mathrm{e}^{-\hat{\Gamma} t}\left[1 + \int_0^t \mathrm{e}^{\hat{\Gamma} t'}\beta(\mathbf{r})\ \zeta(t')\ \mathrm{d}t'\right] \quad (3.7)$$

by using the time-developing operator $\hat{\Gamma}$ defined by

$$\hat{\Gamma} \equiv \dot{\gamma}\hat{P} + \beta(\mathbf{r}) - D\hat{Q} \quad (3.8)$$

The i,j component of the stress as a function of time can then be calculated from the relation[13]

$$\sigma_{i,j}(t) = \int \mathrm{d}\mathbf{r}\ \psi_0(\mathbf{r})(x_i f_j)\ \xi(\mathbf{r}, t) \quad (3.9)$$

To study the short-time behavior, we develop the solution in a power series of time. The formal expansion of the exponential in eq 3.7 in powers of t leads to

$$\xi(\mathbf{r}, t) = 1 + t\xi^{(1)} + \frac{t^2}{2}\xi^{(2)} + \frac{t^3}{3!}\xi^{(3)} + \frac{t^4}{4!}\xi^{(4)} + \cdots \quad (3.10)$$

where

$$\xi^{(1)}(\mathbf{r}) = \dot{\gamma}\Theta(rF) \quad (3.11a)$$

$$\xi^{(2)}(\mathbf{r}) = -\dot{\gamma}\left\{\Theta\left(\hat{c} + \frac{6D}{r^2}\right) + \dot{\gamma}[\Phi^2 + \Theta^2(\hat{p} - 2)]\right\}(rF) \quad (3.11b)$$

$$\xi^{(3)}(\mathbf{r}) = \ddot{\zeta}_0\beta(\mathbf{r}) + \dot{\gamma}\left\{\Theta\left(\hat{c} + \frac{6D}{r^2}\right)^2 + \dot{\gamma}\hat{\Xi}_1 + \dot{\gamma}^2\Theta[3\Phi^2 + \Theta^2(\hat{p} - 4)](\hat{p} - 2)\right\}(rF) \quad (3.11c)$$

$$\xi^{(4)}(\mathbf{r}) = \dddot{\zeta}_0\beta(\mathbf{r}) - \dot{\gamma}\left\{\Theta\left(\hat{c} + \frac{6D}{r^2}\right)^3 + \dot{\gamma}\hat{\Xi}_2 + \dot{\gamma}^2\hat{\Xi}_3 - \dot{\gamma}^3[3\Phi^4 + 6\Phi^2\Theta^2(\hat{p} - 4) + \Theta^4(\hat{p} - 6)(\hat{p} - 4)](\hat{p} - 2)\right\}(rF) \quad (3.11d)$$

In these equations, angular factors $\Theta(\theta, \phi)$ and $\Phi(\theta, \phi)$ are separated as the prefactors of the radial differencial operators $\hat{c}, \hat{p}$, and so forth on moving to spherical coordinates. Definitions of operators $\hat{\Xi}_1 \sim \hat{\Xi}_3$ and of angular factors Θ,Φ together with radial operators $\hat{c}, \hat{p}$ are described in detail in Appendix A.

4. Shear Stress

We first study the shear stress $\sigma_{x,y}(t)$ as a function of time. Because it is on the order of $\dot{\gamma}$, the shear viscosity buildup function

$$\eta^+(t) \equiv \sigma_{x,y}(t)/\dot{\gamma} \quad (4.1)$$

is commonly used. Substituting the expansion (eq 3.10) into the stress equation (eq 3.9) and integrating over all possible end-to-end vectors, we find

$$\eta^+(t) = t\eta^{(1)} + \frac{t^2}{2}\eta^{(2)} + \frac{t^3}{3!}\eta^{(3)} + \frac{t^4}{4!}\eta^{(4)} + \cdots \quad (4.2)$$

The first term is given by

$$\eta^{(1)} = c_{2,0}a_1 \quad (4.3)$$

after integration, where the numerical coefficient

$$c_{2,0} \equiv \int \sin\theta\ \mathrm{d}\theta\ \mathrm{d}\phi\ \Theta^2 = \frac{4\pi}{15} \quad (4.4)$$

appears from the angular integral and the main part

$$a_1 \equiv \int_0^l \mathrm{d}r\ \psi_0(r)(r^4 fF) \quad (4.5)$$

appears from the radial integration. In TK, we found that the high-frequency limit of the storage modulus is given by the same integral.[26] Hence, we confirm that the initial slope of

(26) The integral a_1 was named a_2 in TK. In this article, we rename all integrals so that the numbers attached to them coincide with the sequence in which they appear.

the viscosity growth function is given by the high-frequency modulus

$$\eta^{(1)} = \lim_{\omega\to\infty} G'(\omega) = \frac{4\pi}{15} a_1 \equiv g_1 \tag{4.6}$$

as it should.

The second term is given by

$$\eta^{(2)} = -c_{2,0}(b_1 + Da_2) \tag{4.7}$$

where

$$b_1 \equiv \int_0^l \mathrm{d}r\, \psi_0(r)(r^4 \beta f F) \tag{4.8}$$

and

$$a_2 \equiv \int_0^l \mathrm{d}r\, \psi_0(r)(r^4 f F)\left[\left(\frac{1}{r} + \frac{f'}{f}\right)\left(\frac{1}{r} + \frac{F'}{F}\right) + \frac{6}{r^2}\right] \tag{4.9}$$

In TK, we found that the slope of loss modulus is given by the same integral in the limit of high frequency. We thus find a new result

$$\eta^{(2)} = -\lim_{\omega\to\infty} \omega G''(\omega) \equiv -g_2 \tag{4.10}$$

where

$$g_2 \equiv \frac{4\pi}{15}(b_1 + Da_2) \tag{4.11}$$

The coefficient $\eta^{(2)}$ is negative definite, and independent of the shear rate. Also, it is clear that the nonaffine diffusion term Da_2 makes a negative contribution to the second coefficient. If the junctions are allowed to diffuse around the mean position without affiness constraint, then the stress is reduced in proportion to the diffusion coefficient D of the micellar junction. The specific values of g_1 and g_2 depend upon the chain property (in particular, amplitude A), and the coupling constant g through $\beta(r)$ in eq 2.6.

The third term can be written in the form

$$\eta^{(3)} = Q_0 + Q_2\dot{\gamma}^2 \tag{4.12}$$

where

$$Q_0 = c_{2,0}(b_2 + Db_3 + D^2 b_4) \tag{4.13a}$$

and

$$Q_2 = 3c_{2,2}a_3 - c_{4,0}a_4 = \frac{1}{3}c_{2,2}a_8 \tag{4.13b}$$

Coefficients c are defined by the angular integrals

$$c_{2,2} \equiv \int \sin\theta\, \mathrm{d}\theta\, \mathrm{d}\phi\, \Theta^2\Phi^2 = \frac{4\pi}{35} \tag{4.14a}$$

and

$$c_{4,0} \equiv \int \sin\theta\, \mathrm{d}\theta\, \mathrm{d}\phi\, \Theta^4 = \frac{4\pi}{105} = \frac{1}{3}c_{2,2} \tag{4.14b}$$

Radial integrals a,b are explicitly given in the list in Appendix B. In the particular case of an affine network with $D = 0$, we find

$$\eta^{(3)} = \frac{4\pi}{15}\left(b_2 + \frac{1}{7}a_8\dot{\gamma}^2\right) \tag{4.15}$$

4.1. Strain Hardening. We have derived the power expansion in the form

$$\eta^+(t) = g_1 t - \frac{g_2}{2}t^2 + \frac{1}{6}(Q_0 + Q_2\dot{\gamma}^2)t^3 + \cdots \tag{4.16}$$

up to third order. It is an alternating power series, so the long-time behavior is difficult to predict. However, we can discuss how the nonlinear effect takes place up to this order. Let us first examine the sign of this third coefficient. If it is negative, then the viscosity decreases as time goes on. If it is positive, then the viscosity may deviate upward from the baseline $\eta^+(t) = g_1 t$ fixed by the linear modulus. In other words, at a certain time it shows an upturn from the linear baseline. Such stress growth exceeding the linear baseline by a large deformation is called strain hardening.

Figure 3a,b schematically shows the relationship among strain hardening, stress overshoot, and steady nonlinear viscosity in the shear-thinning regime. For a sufficiently high shear rate, the viscosity first shows an upward deviation due to strain hardening, followed by the overshoot peak, and then it asymptotically decreases to the stationary value. Strain hardening is caused by the stretching of the chains beyond the linear regime before the end groups are dissociated. It is therefore nonlinear behavior that cannot be observed for Gaussian chains. Such nonlinear stretching is often seen in the stress−strain curve of natural rubbers in the high-elongation region where subchains in the networks are overstretched. There has been, however, no experimental report on strain hardening in polymer solutions and melts. The entanglements may therefore be capable of causing stress overshoot but may not be strong enough to cause hardening. The transient network that we study here lies somewhere between them. To show the relationship between the initial stress growth and the long-time asymptotic behavior, the stationary viscosity is plotted in Figure 3b.

Let us find the critical shear rate $\dot{\gamma}$ at which strain hardening starts to appear. It can be found by the condition

$$-g_2 + \frac{1}{3}(Q_0 + Q_2\dot{\gamma}^2)t = 0 \tag{4.17}$$

for the cancelation of the second and third terms.

In Figure 4a, we show the exact numerical calculation of the solutions of the TE equation. (In what follows, the numerical values of the stresses are presented in units of $\nu k_B T$). The shear rate $\dot{\gamma}$ is varied from curve to curve. The number of statistical units on the chain is assumed to be $n = 20$, and the coupling constant in the dissociation rate is fixed at $g = 0.2$. In Figure 4b, the linear baseline $g_1 t$ is subtracted from each curve of $\eta^+(t)$, and the results are shown as broken lines.

To examine the accuracy of the power series in eq 4.16 up to the third order, we carry out the same procedure for eq 4.16 and show $-g_2 t^2/2 + (Q_0 + Q_2\dot{\gamma}^2)t^3/6$ by solid lines in the same Figure. We can see the change in the sign of the slope around $t \simeq 0.1$, which decides the occurrence of hardening. Therefore, we put $t = 0.1$ in the hardening condition (eq 4.17) and solve it for $\dot{\gamma}$ to find the critical shear rate $\dot{\gamma}_c$ for hardening. The result is

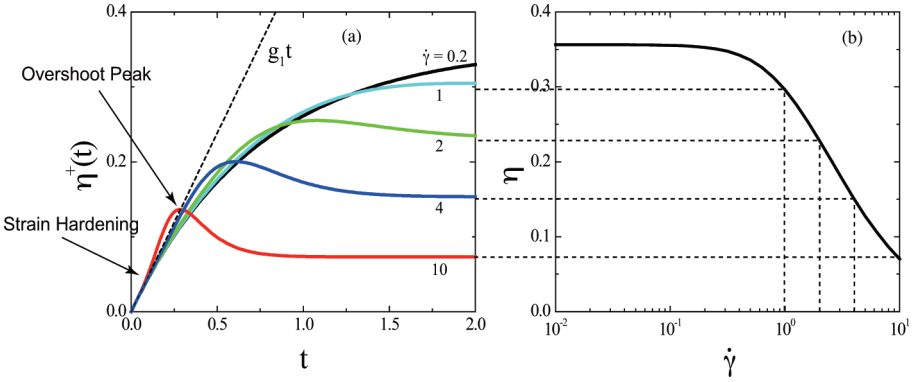

Figure 3. Concepts of strain hardening, stress overshoot, and the nonlinear stationary viscosity are shown by taking typical theoretical results of the stress buildup function. (a) Time development of the viscosity for different shear rates. The initial slope is given by the linear storage modulus. The linear baseline (---) is defined by $\eta^+(t) = g_1 t$. For large $\dot\gamma$, the viscosity shows hardening and overshoot. (b) Nonlinear stationary viscosity plotted as a function of the shear rate.

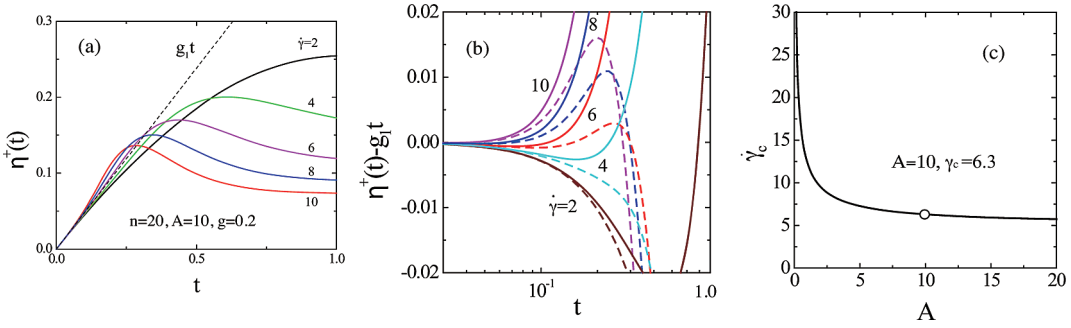

Figure 4. (a) Growth curves of the viscosity numerically calculated for the TE affine transient network equation (eq 3.7) with $D = 0$. The shear rate $\dot\gamma$ is changed from curve to curve for a nonlinear chain with $A = 10$. (b) Deviation $\eta^+(t) - g_1 t$ of the viscosity from the reference baseline defined by the linear modulus plotted against time (---) and the same for the third-order approximation (eq 4.16). (c) Critical shear rate $\dot\gamma_c$ for the appearance of strain hardening found by eq 4.17 plotted against the nonlinear amplitude A of the tension−elongation curve of a polymer chain. The higher the nonlinearity of the chain, the easier the strain hardening.

plotted against the nonlinear amplitude A in Figure 4c. Gaussian chains ($A = 0$) do not show any hardening. For a nonlinear chain with $A = 10$, for instance, the critical value obtained in this way is $\dot\gamma_c = 6.3$. It agrees well with the exact numerical solution. Thus, it turns out that the method of expansion in powers of time gives a sufficiently precise solution as far as the critical shear rate is concerned. In addition, it provides a method to study non-affine diffusion of the junctions.

4.2. Stress Overshoot. Let us study next the overshoot in the shear stress. For polymer solutions and melts, it is often claimed that the deformation $\gamma_{max} \equiv \dot\gamma t_{max}$ accumulated before the stress reaches the maximum is independent of the shear rate and takes a value on the order of unity (1.0 in the literature[27]). In other publications,[28,29] it depends on the shear rate and is approximately described by the formula $\gamma_{max} \equiv a[b + (\dot\gamma\tau)^{2/3}]^{3/2}$, where a and b are numerical constants on the order of unity and τ is the relaxation time. Recent studies[30,31] of entangled solutions and melts suggest that the stress overshoot corresponds to the yield point of the entangled network and that the characteristics of the yield point obey universal scaling laws.

In gelling solutions, γ_{max} seems to depend on the system. For aqueous solutions of guar galactomannan[32] at 3 wt %, $\gamma_{max} \simeq 2$, whereas in aqueous solutions of xanthan polysaccharides[33] at 2 wt % it increases with the shear rate from 0.5 to 1.0. Because the results are scattered depending on the system under study and also the origin of the overshoot has not been clarified, analysis on the basis of a molecular model capable of quantitative predictions as presented in this article is very important.

For the transient networks in the present study, it is very probable that the stress shows a maximum at a certain time t_{max} in the regime where strain hardening occurs but it may show a maximum even in the regime where there is no strain hardening, as reflected by the curves for small $\dot\gamma$ in Figure 4a. We therefore first carried out a numerical integration of the TE equation by using different values A of chain nonlinearity for a fixed coupling constant $g = 0.2$ and found t_{max} as a function of $\dot\gamma$. The results are shown in Figure 5. We can see that the accumulated deformation γ_{max} is almost independent of the shear rate for both Gaussian ($A = 0$) and nonlinear ($A = 10$) chains (Figure 5b). The viscosity $\eta_{max} \equiv \eta(t_{max})$ at the maximum time decreases with the shear rate (Figure 5c).

To understand the condition for overshooting in terms of molecular characteristics, we study the stress buildup curve corresponding to eq 4.16 in detail. Unfortunately, the terms up to the third order of time turn out to be insufficient to find the peak position because the $O(t^3)$ term is definitely positive. Therefore, we calculated the $O(t^4)$ terms in the special case of $D = 0$ (affine network). We found that the power series has

(27) Menedes, E. V.; Graessley, W. W. *Rheol. Acta* **1980**, *19*, 38.
(28) Pearson, D.; Herbolzheimer, E.; Grizzuti, N.; Marrucci, G. *J. Polym. Sci., Part B: Polym. Phys.* **1991**, *29*, 1589.
(29) Osaki, K.; Inoue, T.; Isomura, T. *J. Polym. Sci., Part B: Polym. Phys.* **2000**, *38*, 1917.
(30) Wang, S.-Q.; Ravindranath, S.; Wang, Y.; Boukany, P. *J. Chem. Phys.* **2007**, *127*, 064903.
(31) Ravindranath, S.; Wang, S.-Q. *J. Rheol.* **2008**, *52*, 681.
(32) Richardson, R. K.; Ross-Murphy, S. B. *Int. J. Biol. Macromol.* **1987**, *9*, 249.
(33) Richardson, R. K.; Ross-Murphy, S. B. *Int. J. Biol. Macromol.* **1987**, *9*, 257.

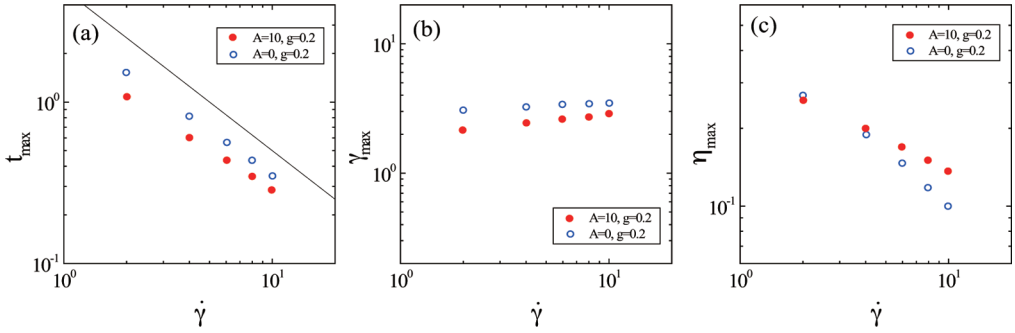

Figure 5. Numerical calculation of TE model (affine network) with $g = 0.2$ for the chain and $A = 0, 10$ with $n = 20$. (a) Overshoot time t_{max}, (b) accumulated deformation γ_{max}, and (c) viscosity at the maximum time, all plotted against the shear rate.

alternating signs in the form of

$$\eta^+(t) = g_1 t - \frac{g_2}{2}t^2 + \frac{g_3(\dot\gamma)}{6}t^3 - \cdots + \frac{g_{2n-1}(\dot\gamma)}{(2n-1)!}t^{2n-1} - \frac{g_{2n}(\dot\gamma)}{(2n)!}t^{2n} + \cdots \quad (4.18)$$

where the coefficients take the form of

$$g_{2n-1}(\dot\gamma) = Q_0^{(2n-1)} + \cdots + Q_{2n-2}^{(2n-1)}\dot\gamma^{2n-2} \quad (4.19a)$$

$$g_{2n}(\dot\gamma) = Q_0^{(2n)} + \cdots + Q_{2n-2}^{(2n)}\dot\gamma^{2n-2} \quad (4.19b)$$

as functions of the shear rate. Then, the time derivative takes the form of

$$\frac{d\eta^+(t)}{dt} = g_1 - g_2 t + \frac{g_3}{6}t^3 + \cdots + \frac{g_{2n-1}}{(2n-2)!}t^{2n-2} - \frac{g_{2n}}{(2n-1)!}t^{2n-1} + \cdots \quad (4.20)$$

In the limit of high shear rate $\dot\gamma$, the dominant term is the one with the highest power of time. All intermediate terms cancel alternatively, and the peak appears when the first term is balanced by the last term, i.e., when the condition

$$\frac{g_{2n}}{(2n-1)!}t^{2n-1} \simeq g_1 \quad (4.21)$$

is fulfilled. Hence, we have $t_{max}^{2n-1} \simeq (2n-1)!g_1/g_{2n} \simeq (2n-1)!g_1/Q_{2n-2}^{(2n)}\dot\gamma^{2n-2} \simeq \dot\gamma^{-(2n-2)}$. The peak time is therefore given by

$$t_{max} \simeq \dot\gamma^{-(2n-2)/(2n-1)} \simeq \dot\gamma^{-1} \quad (4.22)$$

for large n. Hence, we expect that the accumulated deformation is asymptotically independent of the shear rate and is given as a function of the coupling constant g and the nonlinearity A.

To clarify how the accumulated deformation depends upon the shear rate in nonaffine networks, we have carried out a molecular dynamics simulation by using the same bead−spring model for polymer chains as in our previous study.[34] Beads are connected by the finitely extensible nonlinear elastic springs. Each chain carries end beads interacting with cross-linkers through an associative potential. Details of the simulation will be reported elsewhere. The overshoot time, the total deformation before the overshoot time, and the maximum stress are shown in Figure 6. We found that the overshoot starts to appear at a finite shear rate on the order of unity. The peak time is inversely proportional to the shear rate. The accumulated deformation obeys the law $\gamma_{max} \simeq 3.0$ and increases weakly with the shear rate.

5. Normal Stress Differences

Let us next briefly study the normal stresses. The first and second normal stress differences are defined by

$$N_1^+(t) = \sigma_{x,x} - \sigma_{y,y} \quad (5.1a)$$

and

$$N_2^+(t) = \sigma_{y,y} - \sigma_{z,z} \quad (5.1b)$$

Because they are of order $O(\dot\gamma^2)$, data are conventionally recorded in the form of the normal stress coefficients

$$\Psi_i^+(t) \equiv N_i^+(t)/\dot\gamma^2 \quad (5.2)$$

for $i = 1$ and 2. By substitution of the power expansion (eq 3.10), we find

$$\Psi_i^+(t) = \frac{t^2}{2}\psi_i^{(2)} + \frac{t^3}{3!}\psi_i^{(3)} + \frac{t^4}{4!}\psi_i^{(4)} + \cdots \quad (5.3)$$

Both start from $O(t^2)$.

5.1. First Normal Stress Difference. Upon substitution of $\xi^{(2)}$, we find that the second term is given by

$$\psi_1^{(2)} = 2c_{2,0}a_1 = 2G'(\omega = \infty) = 2g_1 \quad (5.4)$$

which is twice as large as the initial slope of the shear stress. After straightforward but tedious calculations, we find the higher terms to be

$$\psi_1^{(3)} = -4g_2 - D[(\lambda_{0,2}^{(1)} - 12c_{2,0})a_6 - \lambda_{2,0}^{(1)}a_7] \quad (5.5)$$

and

$$\psi_1^{(4)} = -(S_{1,0} + S_{1,2}\dot\gamma^2) \quad (5.6)$$

where

$$S_{1,0} = 3c_{0,2}^{(1)}[b_2 + Db_5^{(1)} + D^2b_6^{(1)}] - 3c_{2,0}^{(1)}b_6 \quad (5.7a)$$

and

$$S_{1,2} = -3c_{0,4}^{(1)}a_3 + 6c_{2,2}^{(1)}a_4 - c_{4,0}^{(1)}a_9 \quad (5.7b)$$

Numerical coefficients c and λ are defined in Appendix A. Because $c_{2,0}^{(1)} \equiv 0$ by symmetry, the last term in $S_{1,0}$ disappears.

(34) Koga, T.; Tanaka, F. *Eur. Phys. J. E* **2005**, *17*, 115.

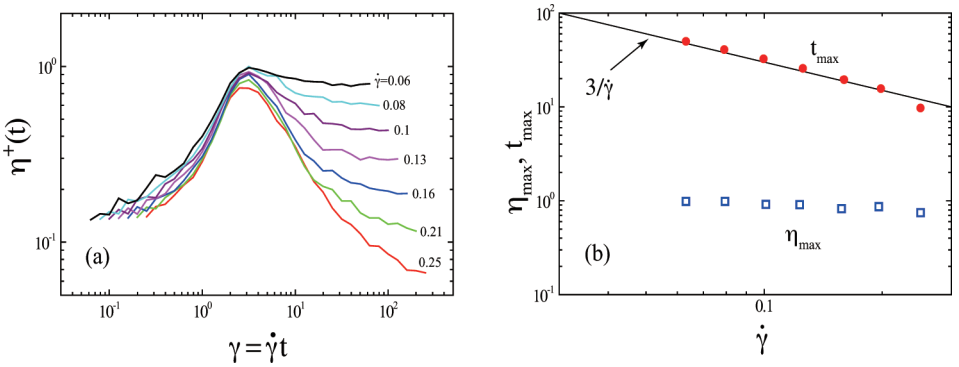

Figure 6. Stress overshoot studied by molecular dynamics simulation. (a) Time-dependent viscosity plotted against deformation. All of the curves coincide near the maximum. (b) The time t_{max} at which the shear stress shows a maximum and the peak value η_{max} at the maximum is plotted against the shear rate. The accumulated deformation γ_{max} before the stress is almost independent of the shear rate and is given by $\gamma_{max} \simeq 3.0$.

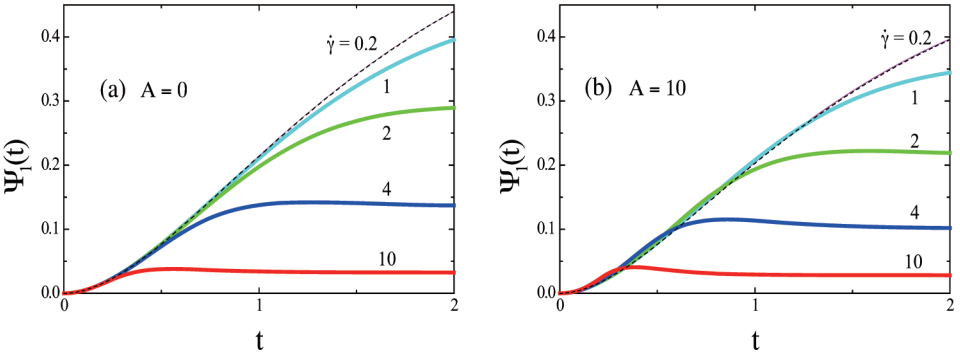

Figure 7. First normal stress difference numerically calculated for the TE model with $g = 0.2$ for the chain with $n = 20$. (a) $A = 0$ (Gaussian) and (b) $A = 10$.

As for $S_{1,2}$, because the coefficient $c^{(1)}_{4,0} \equiv 0$ again by symmetry, the last term disappears. The other terms incidentally vanish for the Gaussian chain ($A = 0$), but for the nonlinear chain, they can be the origin of hardening in the first normal stress just as in shear stress. Because the effect of diffusion in the normal stresses is beyond the scope of the present study, we do not show the explicit forms of integrals $b^{(1)}_i$ and $b^{(2)}_i$ in the following section.

5.2. Second Normal Stress Difference. Similarly, we find

$$\psi_2^{(2)} = -c^{(2)}_{2,0} a_{10} \tag{5.8}$$

for the second normal stress coefficient. Integral a_{10} is explicitly given in Appendix B. It vanishes for a Gaussian chain but takes a negative value for a nonlinear chain with $A > 0$ so that the initial slope of the second normal stress difference is positive (Figure 8a,b).

We also find for higher-order terms

$$\psi_2^{(3)} = 4g_2 + c^{(2)}_{2,0}(-2a_3 + b_5) - D[(\lambda^{(2)}_{0,2} - 12c_{2,0})a_6 - \lambda^{(2)}_{2,0} a_7] \tag{5.9}$$

and

$$\psi_2^{(4)} = -(S_{2,0} + S_{2,2}\dot\gamma^2) \tag{5.10}$$

where the coefficients S are given by

$$S_{2,0} = 3c^{(2)}_{0,2}[b_2 + Db^{(2)}_5 + D^2 b^{(2)}_6] - 3c^{(2)}_{2,0} b_6 \tag{5.11a}$$

and

$$S_{2,2} = -3c^{(2)}_{0,4} a_3 + 6c^{(2)}_{2,2} a_4 - c^{(2)}_{4,0} a_9 \tag{5.11b}$$

Numerical coefficients c and λ are defined in Appendix B. In the fourth-order term, $S_{2,0} > 0$ for $D = 0$ and $S_{2,2} > 0$ except for Gaussian chains so that an overshoot appears in the second normal stress as in the shear stress.

In the earlier study of TE, it was found, for a special model of the dissociation rate, that an overshoot appears in the sequence of shear, first normal, and second normal stress. On the basis of the phenomenological constitutional equation, Yamamoto[35] estimated that the peak time t^{n1}_{max} of the first normal stress in a polymer melt is twice as large as the peak time t^{s}_{max} of the shear stress. From the numerical calculation of the present molecular model, we find $t^{n1}_{max} < 2t^{s}_{max}$. In other words, the first normal stress reaches the peak earlier than predicted by the phenomenology.

Moreover, by close observation of the buildup curves of the second normal stress difference in Figure 8b, one finds that its stationary value changes sign from positive to negative with increasing shear rate. Consequently, curves with high values of $\dot\gamma$ exhibit an undershoot after passing the peak.

6. Experimental Section

To examine the validity of the theoretical prediction presented above, we have experimentally studied the rheological properties of HEUR aqueous solutions. We used HEUR with a poly (ethylene oxide) (PEO) main chain with each end capped with a

(35) Yamamoto, M. *Trans. Soc. Rheol.* **1971**, *15*, 331.

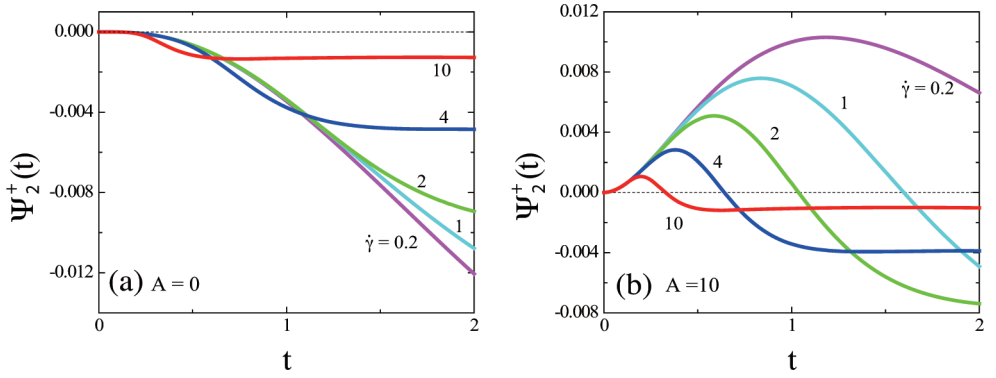

Figure 8. Second normal stress difference calculated for the TE model with $g = 0.2$ and $n = 20$. (a) $A = 0$ and (b) $A = 10$.

2-decyl-tetradecyl chain through a urethane linker (referred to as C24-HEUR, see Figure 9).[36,37] The polymer was synthesized by a condensation reaction using PEO chains ($M_w \simeq 11\,000$ g mol^{-1}). The weight-average molecular weight (M_w) of the polymer was 27 000 g mol^{-1}, and the polydispersity index M_w/M_n was 2.5.[36] According to GPC measurements, the sample used contains polymers consisting of several primary PEO chains (one to three chains). The effect of polydispersity on the degree of polymerization will be discussed in section 7.2.

Rheological measurements were conducted with a rheometer (RDA II, Rheometrics) in parallel-plate geometry. The plate radius was 25 mm, and the gap between the plates was 1.5 mm. The storage and loss moduli were measured as functions of angular frequency ω. In the start-up experiments, a constant shear rate of 1−100 s^{-1} was applied to the solution, and the stress was recorded as a function of time. Measurements were carried out at 22 ± 1 °C with 2 to 3 wt % C24-HEUR aqueous solutions. The concentration range covered in this study is well beyond the gelation threshold concentration[36] (≃0.4 wt %). Therefore, transient networks are expected to be formed in the solutions under the condition of the present study.

The storage and loss moduli, $G'(\omega)$ and $G''(\omega)$, respectively, for a 2 wt % C24-HEUR solution are shown in Figure 10, together with the theoretical fitting curves described in the following text.

Figure 11 shows the time dependence of the shear stress obtained by start-up experiments. At low shear rates $\dot{\gamma} < 1$ s^{-1} lying in the Newtonian regime, the stress first increases linearly with time obeying the first term in eq 4.16 and then saturates to its stationary value. The solid line in Figure 11a is the stress growth function of the hypothetical Maxwell model with strength G'_∞ and a relaxation time τ determined below. The experimental stress growth function in the Newtonian regime (small $\dot{\gamma}$) is well described by this Maxwell model.

In the shear-thinning regime, the stress growth function deviates substantially from that of the Maxwell model for high shear rates ($\dot{\gamma} \geq 1$ s^{-1}). The stress increases linearly in the short-time region of $t < 5$ s and then goes through a maximum, followed by a gradual decrease toward the stationary value. For larger shear rates $\dot{\gamma} \geq 7$ s^{-1}, the increase in the stress is steeper than the linear growth. This corresponds to the strain hardening predicted by the theory.

The measurements were very reproducible; strain hardening (upturn of the stress) was observed repeatedly. Therefore, these observations cannot be ascribed to wall slip, which may lead to occasional abnormal values. The characteristic stress growth reported here has an intrinsic molecular origin, such as chain stretching.

Figure 12 shows the experimental data of the shear-rate-dependent stationary viscosity $\eta(\dot{\gamma})$ and linear oscillatory viscosity $\eta^*(\omega)$, together with the theoretical fitting curve. We can see that,

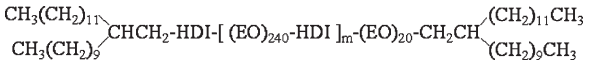

Figure 9. Chemical structure of C24-HEUR. (HDI is hexamethylene diisocyanate.)

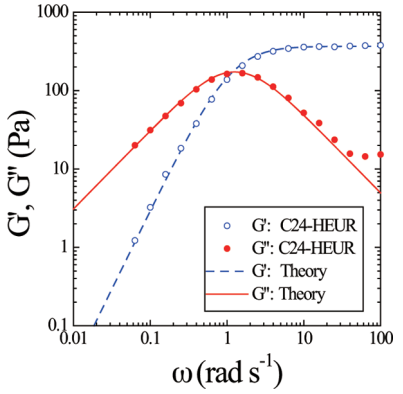

Figure 10. Comparison between theory (lines) and experimental data (circles) for the complex moduli of the C24-HEUR aqueous solution of 2 wt %.

in the shear thinning region in the present study, these two agree with each other so that the Cox−Merz rule holds.

7. Comparison with Experiments

7.1. Evaluation of the Theoretical Parameters. In this section, we make quantitative comparisons between theory and experiment. We first estimate the parameters used in the theory from the molecular properties and the experimental conditions.

The number of segments of the PEO main chain is estimated to be $n = 320$ on the basis of the literature value[38] of the Kuhn length $a = 0.7$ nm and the length of a monomeric unit $a_0 = 0.36$ nm. From the polymer concentration $c = 2$ wt % and the molecular weight $M_w = 27\,000$ g mol^{-1}, the number density ν of polymers is

$$\nu = \frac{cN_A}{M_w} = 4.46 \times 10^{23}\ \mathrm{m}^{-3} \tag{7.1}$$

In the case of $T = 295$ K, we then have

$$\nu k_B T = 1816\ \mathrm{Pa} \tag{7.2}$$

For parameter A characterizing the nonlinearity in the chain tension, we fitted eq 2.5 to the data of the tension−elongation

(36) Yoshida, K.; Nakamura, A.; Nakajima, Y.; Fukuhara, T.; Inoue, H.; Kaneda, I. *IFSCC Mag.* **2007**, *10*, 2.
(37) Kaneda, I.; Koga, T.; Tanaka, F. *Prog. Colloid Polm. Sci.*, 2009, in press.
(38) Oesterhelt, F.; Rief, M.; Gaub, H. E. *New J. Phys.* **1999**, *1*, 61.

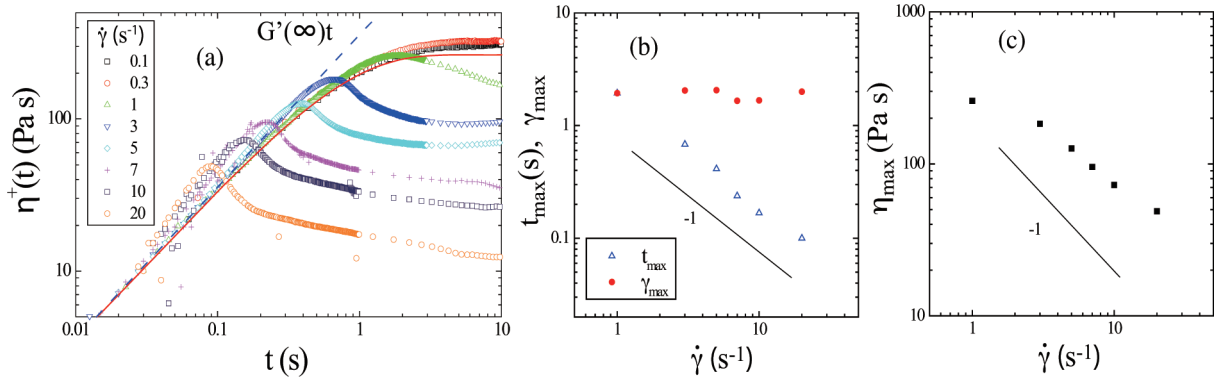

Figure 11. (a) Stress growth function for a C24-HEUR aqueous solution of 2 wt %. The solid line shows the baseline of the hypothetical Maxwell model with a single relaxation time. The broken line represents the expected initial slope $G'(\infty)$ of the stress growth function. (b) Plots of the overshoot time t_{max} (triangles) and the total deformation γ_{max} accumulated before the peak (circles) as functions of shear rate. (c) Peak value η_{max} of the viscosity (squares) plotted against the shear rate.

curve obtained directly by AFM measurement[38] and found A = 5 for the optimal value.

The molecular weight of PEO used here lies below the threshold of the entanglement. A 1% solution of the homopolymer counterpart has a very low viscosity. Hence, entanglements do not play a major role in stress buildup in our measurements.

We next determined the parameters β_0, g, and α by fitting the theoretical curves of the linear viscoelasticity and of the steady shear viscosity with the experimental data. We found

$$\beta_0 = 0.47\ \mathrm{s}^{-1} \tag{7.3}$$

$$g = 35 \tag{7.4}$$

$$\alpha = 0.3\ \mathrm{s}^{-1} \tag{7.5}$$

by optimization. The fitted results are shown in Figures 10 and 12. Both the linear moduli and the nonlinear stationary viscosity are well described by the theory. We found the relaxation time τ = 0.79 s and the modulus G''_∞ = 367 Pa from the peak position of G'' in Figure 10. These values are used for the hypothetical Maxwell model described above to draw the baseline in Figure 11. Because the theoretical fitting curves in Figure 10 and 12 are calculated on the basis of TE with a tension-dependent dissociation rate of eq 2.6, they are different from those based on this hypothetical Maxwell model with a single relaxation time. We also obtained the fraction of the number of elastically effective chains to be ν_e/ν = 0.27. This means that a quarter of the total polymer chains act as bridge chains.

7.2. Stress Growth. Having precisely fixed the three necessary theoretical parameters as described above, we can calculate the stress as a function of time. Figure 13 compares the theoretical curves with the experimental data. For a small shear rate of $\dot\gamma$ = 1 s^{-1}, the theory agrees well with the experiments as shown in Figure 13a. For large shear rates, however, the time evolution of the stress obtained by the theory becomes slower than the experimental data as shown in Figure 13b. In particular, the overshoot peak time predicted by the theory is about twice as large as that of the experiment. In addition, the stress upturn is underestimated by the theory.

We found that the discrepancy can be reduced by using a larger value of A. However, we need extremely large values of A, larger than 1000, to get a good fit. Such a large value of A is not

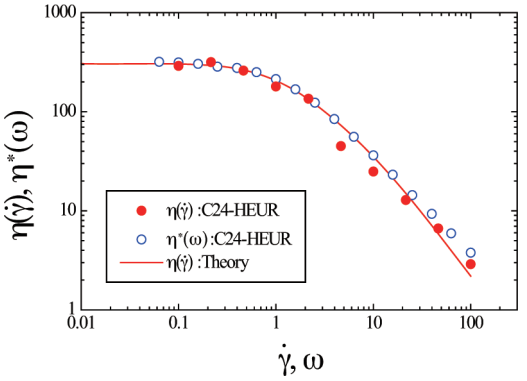

Figure 12. Theoretical calculation (line) and the experimental data (black circles) of the steady shear viscosity $\eta(\dot\gamma)$ for a 2 wt % C24-HEUR aqueous solution. The experimental data of the complex linear viscosity $\eta^*(\omega)$ (white circles) are also shown for reference.

realistic because tension−elongation curve eq 2.5 measured by AFM experiment[38] indicates a much lower value of A.

To explain such a discrepancy, we consider the effect of polydispersity on the degree of polymerization. On the basis of GPC data, it is estimated that the sample used in this study contains polymers with m = 1, 2, and 3 (chemical structural formula in Figure 9). Because the average molecular weight M_w = 27 000 g mol^{-1} is close to that of polymers with m = 2, there must be a large number of short chains with $M_w/2$ in the solution tested in the rheology experiments.

In the linear regime where dynamic mechanical moduli are measured, polydispersity does not affect the results significantly because the chains are not stretched. Therefore, we expect good agreement between theory and experiment. However, in the nonlinear regime such as seen in hardening and overshoot, chain stretching is important.

Shorter chains are easily stretched to the nonlinear regime by smaller elongation, and hence for short chains, dissociation takes place more frequently than for longer ones. Consequently, the time when the stress upturn starts and the time when the stress reaches a peak (overshoot time) are expected to become shorter if short chains are mixed with longer ones.

The present theoretical model for monodisperse chains works well to describe the rheology of systems in the linear regime where chains experience only small deformations around the equilibrium conformation, as seen in Figure 10 in the case of the dynamic mechanical moduli. In the nonlinear regime where

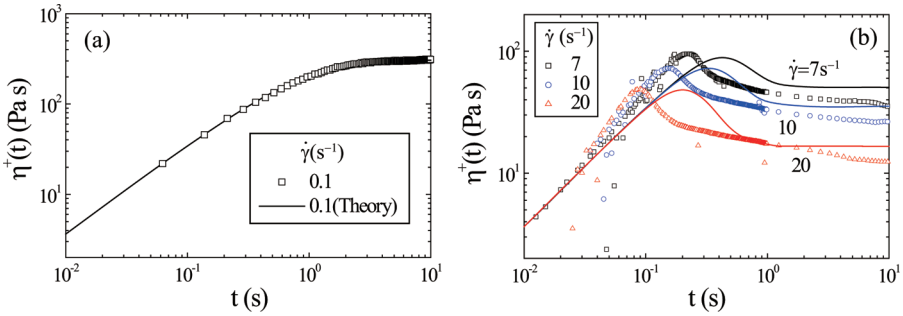

Figure 13. Stress growth function as compared between theory and experiment for a 2 wt % C24-HEUR aqueous solution. (a) Newtonian regime of small $\dot{\gamma}$, (b) Shear thinning regime of larger $\dot{\gamma}$.

chains are highly stretched, however, polydispersity affects the results significantly. Polydispersity can be incorporated into the model, but at the expense of more cumbersome notations. This was not done in the present stage of study.

For a quantitative discussion, we estimate the time t_L required for a polymer chain with n to be stretched to its total length $L = na$. Let R_0 be the end-to-end distance of the polymer chain in the quiescent state $\dot{\gamma} = 0$. The strain $\gamma_L \equiv \dot{\gamma} t_L$ required for the chain to be stretched from R_0 to the full length L under shear deformation is given by

$$\gamma_L^2 = \frac{L^2}{R_0^2} - 1 \simeq \frac{L^2}{R_0^2} \tag{7.6}$$

The ratio of γ_L for polymer chains with n_1 and n_2 is therefore given by

$$\frac{\gamma_{L2}}{\gamma_{L1}} \simeq \frac{L_2}{L_1} \tag{7.7}$$

This gives the ratio of time t_L as

$$\frac{t_{L2}}{t_{L1}} \simeq \frac{L_2}{L_1} = \frac{n_2}{n_1} \tag{7.8}$$

Hence, if $n_2 = n_1/2$, we find $t_{L2} = t_{L1}/2$. Because the overshoot time is considered to be estimated by the elongation time t_L, the discrepancy between theory and experiment shown in Figure 13b can be explained by the effect of short chains.

8. Conclusions and Discussion

We have studied time-dependent stresses in start-up shear flows on the basis of the affine (and nonaffine whenever the calculation is feasible) transient network theory. We paid special attention to the nonlinear phenomena of strain hardening and the overshoot maximum in the shear stress. This model offers major advantages in describing the time-dependent rheology of self-assembled transient networks of hydrophobically modified water-soluble polymers in that it can clarify the relationship between the molecular parameters of a polymer chain and the macroscopic rheological properties of the network under flow beyond the linear regime.

By an expansion in powers of time, the critical shear rate $\dot{\gamma}_c(g, A)$ for the occurrence of strain hardening is found to be a function of the tension-dissociation coupling constant g of the bridge chains and the nonlinearity amplitude A in the tension. Amplitude A significantly affects the nonlinear rheology in the high-chain-stretching region. Time $t_{max}(\dot{\gamma}, g, A)$ when the shear stress shows a maximum peak in the overshooting behavior is also found as a function of the shear rate $\dot{\gamma}$, the coupling constant g, and the amplitude A. The total deformation $\gamma_{max} \equiv \dot{\gamma} t_{max}$ that accumulates before the stress reaches the maximum turns out to depend very weakly upon the shear rate and is practically given by the numerical value on the order of unity. To confirm the results, exact numerical integrations of the affine network model were also carried out.

The model described here, which incorporates nonlinear chain stretching, is very different from the Maxwell model. The two models lead to almost the same result as far as the linear complex moduli are concerned, but the Maxwell model fails to describe nonlinear, phenomena. It predicts neither strain hardening nor overshoot nor shear thickening. This is one of the main reasons that we published this report.

Because our results are directly applicable to water-soluble polymers, we carried out rheological experiments with aqueous solutions of HEUR (telechelic hydrophobically modified PEO) with branched end-chains and made a detailed comparison of theory-derived parameters with the experimental data. The observed experimental time-dependent rheological properties are well understood on the basis of the present theoretical model. We have successfully described observed strain hardening and stress overshoot by using molecular parameters (such as the nonlinearity of the chain, the tension−elongation coupling, and the association−recombination rate) obtained by fitting linear moduli and steady nonlinear viscosity. We also found that the presence of shorter chains mixed with longer ones has a significant effect on strain hardening and stress overshooting because shorter chains are stretched to the nonlinear regime much earlier than longer chains.

We need a firm theoretical basis for the study of nonlinear rheology such as yield, shear banding, or fracture and use a molecular model rather than a phenomenological one, which, starting from the chain characteristics, is capable of quantitatively predicting the macroscopic properties of the system. The study reported here is the first step toward this ultimate goal.

Further application of the theory will involve (1) a detailed study of the first and second normal stress coefficients, in particular, the sign of the initial slope in the second normal stress coefficient, the sequence in which the three stress components reach the overshoot peak, and the conditions for the undershooting, (2) the effect of nonaffine diffusive motion of the network junctions on the strain hardening and stress overshoot, and (3) the rheological behavior of a transient network under elongational flow. These will be reported in our forthcoming papers.

Acknowledgment. This work is partially supported by a Grant-in-Aid for Scientific Research on Priority Areas "Soft Matter Physics" from the Ministry of Education, Culture,

Sports, Science and Technology of Japan and partially supported by a Grant-in-Aid for Scientific Research (B) from the Japan Society for the Promotion of Science under grant number 19350057. We acknowledge their support.

Appendix A: Expansion of the Distribution Function in Powers of Time

To derive the power expansion, we use polar coordinates ($x = r \sin\theta\cos\phi$, $y = r\sin\theta\sin\phi$, and $z = r\cos\theta$) and split the operator $\hat{Q}$ into radial and angular parts

$$\hat{Q} = \hat{R} + r^{-2}\hat{\Lambda}$$

where

$$\hat{R} \equiv \left(\frac{\partial}{\partial r}\right)^2 - \left[F(r) - \frac{2}{r}\right]\frac{\partial}{\partial r}$$

and

$$\hat{\Lambda} \equiv \frac{1}{\sin\theta}\left[\frac{\partial}{\partial\theta}\sin\theta\frac{\partial}{\partial\theta} + \frac{1}{\sin\theta}\left(\frac{\partial}{\partial\phi}\right)^2\right]$$

is the usual angular part of the Laplacian. We then use abbreviated notation

$$\hat{c} \equiv \beta(\mathbf{r}) - D\hat{R}$$

and

$$\Phi \equiv \sin\theta\sin\phi, \quad \Theta \equiv \sin^2\theta\sin\phi\cos\phi$$

Time-development operator $\hat{\Gamma}$ is given by

$$\hat{\Gamma} = \dot{\gamma}\hat{P} + \hat{c} - Dr^{-2}\hat{\Lambda}$$

Operators $\hat{P}$ and $\hat{c}$ act only on the functions of r. A simple calculation gives

$$\hat{\Gamma}1 = -\dot{\gamma}\Theta(rF) + \beta$$

Similarly we have

$$\hat{\Gamma}\beta = \dot{\gamma}\Theta\hat{p}\beta + \hat{c}\beta$$

where the operator $\hat{p}$ is defined by

$$\hat{p} \equiv r\left(\frac{\mathrm{d}}{\mathrm{d}r} - F(r)\right)$$

One more operation leads to

$$\hat{\Gamma}^2 1 = -\dot{\gamma}^2[\Phi^2 + \Theta^2(\hat{p} - 2)](rF) - \dot{\gamma}\Theta\left[\left(\hat{c} + \frac{6D}{r^2}\right)(rF) - \hat{p}\beta\right] + \hat{c}\beta$$

$$\hat{\Gamma}^2\beta = \dot{\gamma}^2[\Phi^2 + \Theta^2(\hat{p} - 2)](\hat{p}\beta) - \dot{\gamma}\Theta\left[\hat{p}\hat{c}\beta + \left(\hat{c} + \frac{6D}{r^2}\right)(\hat{p}\beta)\right] + \hat{c}^2\beta$$

Repeating similar operations, we find the equations up to $\hat{\Gamma}^4 1$ and $\hat{\Gamma}^4\beta$. By substituting the result into the formal relations

$$\xi^{(1)}(\mathbf{r}) = \zeta_0\beta - \hat{\Gamma}\,1$$

$$\xi^{(2)}(\mathbf{r}) = \hat{\Gamma}^2 1 - \zeta_0\hat{\Gamma}\beta + \dot{\zeta}_0\beta$$

$$\xi^{(3)}(\mathbf{r}) = -\hat{\Gamma}^3 1 + \zeta_0\hat{\Gamma}^2\beta - \dot{\zeta}_0\hat{\Gamma}\beta + \ddot{\zeta}_0\beta$$

$$\xi^{(4)}(\mathbf{r}) = \hat{\Gamma}^4 1 - \zeta_0\hat{\Gamma}^3\beta + \dot{\zeta}_0\hat{\Gamma}^2\beta - \ddot{\zeta}_0\hat{\Gamma}\beta + \dddot{\zeta}_0\beta$$

we find, after lengthy calculation, the result given by eq 3.10 in the text. Operators $\hat{\Xi}$ are defined by

$$\hat{\Xi}_1 \equiv 2\Phi^2\left(\hat{c} + \frac{3D}{r^2}\right) + \Theta^2\left[(\hat{p} - 2)\left(\hat{c} + \frac{6D}{r^2}\right) + \hat{c}(\hat{p} - 2)\right] - \frac{D}{r^2}[\lambda_2 + \lambda_1(\hat{p} - 2)]$$

$$\hat{\Xi}_2 \equiv \Phi^2\left[\left(\hat{c} + \frac{6D}{r^2}\right)^2 + \hat{c}\frac{6D}{r^2}\right] + \Theta^2\left[(\hat{p} - 2)\left(\hat{c} + \frac{6D}{r^2}\right)^2 + \hat{c}(\hat{p} - 2)\left(\hat{c} + \frac{6D}{r^2}\right) - \hat{c}^2(\hat{p} - 2)\right] - \frac{D}{r^2}\left\{[\lambda_2 + \lambda_1(\hat{p} - 2)]\left(\hat{c} + \frac{6D}{r^2}\right) - 2\hat{c}[\lambda_2 + \lambda_1(\hat{p} - 2)]\right\} + [\lambda_2 + \lambda_1(\hat{p} - 2)]\hat{c}\left(\frac{D}{r^2}\right)$$

$$\hat{\Xi}_3 \equiv \Theta\Phi^2\left\{3(\hat{p} - 2)\left(\hat{c} + \frac{6D}{r^2}\right) + (\hat{p} - 2)\hat{c} - \hat{c}(\hat{p} - 2)\right\} + \Theta^3\left\{(\hat{p} - 4)(\hat{p} - 2)\left(\hat{c} + \frac{6D}{r^2}\right) + [(\hat{p} - 4)\hat{c} - \hat{c}(\hat{p} - 4)](\hat{p} - 2)\right\} - \frac{D}{r^2}\{\lambda_2 + (\lambda_1 - 3\lambda_4)(\hat{p} - 2) - \lambda_3(\hat{p} - 4)(\hat{p} - 2)\}$$

where $\lambda_1 \equiv \hat{\Lambda}\Theta^2$, $\lambda_2 \equiv \hat{\Lambda}\Phi^2$, $\lambda_3 \equiv \hat{\Lambda}\Theta^3$, and $\lambda_4 \equiv \hat{\Lambda}\Theta\Phi^2$.

Appendix B: Derivation of the Radial and Angular Integrals

Upon such decomposition, we are led to the two types of angular integrals. Some are defined by

$$c_{l,m} \equiv \int \sin\theta\,\mathrm{d}\theta\,\mathrm{d}\phi\Theta^l\Phi^m$$

$$c^{(1)}_{m,n} \equiv \int \sin\theta\,\mathrm{d}\theta\,\mathrm{d}\phi\,\Theta_1\Theta^m\Phi^n$$

$$c^{(2)}_{m,n} \equiv \int \sin\theta\,\mathrm{d}\theta\,\mathrm{d}\phi\,\Theta_2\Theta^m\Phi^n$$

where $\Theta_1 \equiv \sin^2\theta(1 - 2\sin^2\phi)$ and $\Theta_2 \equiv \sin^2\theta(1 + \sin^2\phi) - 1$.

Others are

$$\lambda^{(1)}_{2,0} \equiv \int \sin\theta \, \mathrm{d}\theta \, \mathrm{d}\phi \, \Theta_1 \hat{\Lambda} \, \Theta^2, \quad \lambda^{(1)}_{0,2} \equiv \int \sin\theta \, \mathrm{d}\theta \, \mathrm{d}\phi \, \Theta_1 \hat{\Lambda} \Phi^2$$

$$\lambda^{(2)}_{2,0} \equiv \int \sin\theta \, \mathrm{d}\theta \, \mathrm{d}\phi \, \Theta_2 \hat{\Lambda} \, \Theta^2, \quad \lambda^{(2)}_{0,2} \equiv \int \sin\theta \, \mathrm{d}\theta \, \mathrm{d}\phi \, \Theta_2 \hat{\Lambda} \Phi^2$$

The numerical constants arising from the angular integrals are

$$c_{2,0} = \frac{4\pi}{15}, \quad c_{2,2} = \frac{4\pi}{35}, \quad c_{4,0} = \frac{4\pi}{105}$$

$$c^{(1)}_{2,0} = 0, \quad c^{(1)}_{0,2} = -\frac{8\pi}{15}, \quad c^{(2)}_{2,0} = \frac{8\pi}{105}, \quad c^{(2)}_{0,2} = \frac{8\pi}{15},$$

$$c^{(1)}_{4,0} = 0, \quad c^{(1)}_{2,2} = -\frac{8\pi}{315}, \quad c^{(1)}_{0,4} = -\frac{16\pi}{35}$$

$$c^{(2)}_{4,0} = \frac{16\pi}{1155}, \quad c^{(2)}_{2,2} = \frac{16\pi}{315}, \quad c^{(2)}_{0,4} = \frac{16\pi}{35}$$

After carrying out all angular integrals, we are left with the radial integrals. Those that are necessary and sufficient to describe the dynamic mechanical moduli up to the first order of the diffusion constant are listed below.

$$a_1 = \int_0^l \mathrm{d}r \, \psi_0(r)(r^4 f F)$$

$$a_2 = \int_0^l \mathrm{d}r \, \psi_0(r)(r^4 f F)\left[\left(\frac{1}{r} + \frac{f'}{f}\right)\left(\frac{1}{r} + \frac{F'}{F}\right) + \frac{6}{r^2}\right]$$

$$a_3 = \int_0^l \mathrm{d}r \, \psi_0(r)(r^5 f F)\left(F + \frac{1}{r} - \frac{F'}{F}\right)$$

$$a_4 = \int_0^l \mathrm{d}r \, \psi_0(r)(r^6 f F)\left(\frac{8}{r} + \frac{f'}{f}\right)\left(F + \frac{1}{r} - \frac{F'}{F}\right)$$

$$a_5 = \int_0^l \mathrm{d}r \, \psi_0(r)(r^4 f F)\left[\left(\frac{1}{r} + \frac{f'}{f}\right)\left(\frac{1}{r} + \frac{F'}{F}\right) + \frac{3}{r^2}\right]$$

$$a_6 = \int_0^l \mathrm{d}r \, \psi_0(r)(r^2 f F)$$

$$a_7 = \int_0^l \mathrm{d}r \, \psi_0(r)(r^3 f F)\left(F + \frac{1}{r} - \frac{F'}{F}\right)$$

$$a_8 = \int_0^l \mathrm{d}r \, \psi_0(r)(r^6 f F)\left(F + \frac{1}{r} - \frac{F'}{F}\right)\left(\frac{f'}{f} - \frac{1}{r}\right)$$

$$a_9 = \int_0^l \mathrm{d}r \, \psi_0(r)(r^7 f F)\left(F + \frac{1}{r} - \frac{F'}{F}\right)\left(\frac{f''}{f} + 19\frac{f'}{rf} + \frac{80}{r^2}\right)$$

$$a_{10} = \int_0^l \mathrm{d}r \, \psi_0(r)(r^5 f F)\left(\frac{F'}{F} - F + \frac{6}{r}\right)$$

$$a_{11} = \int_0^l \mathrm{d}r \, \psi_0(r)(r^7 f F)\left(F + \frac{1}{r} - \frac{F'}{F}\right)\left(3\frac{f''}{f} - 55\frac{f'}{rf} + \frac{2470}{11}\frac{1}{r^2}\right)$$

$$b_1 = \int_0^l \mathrm{d}r \, \psi_0(r)(r^4 \beta f F)$$

$$b_2 = \int_0^l \mathrm{d}r \, \psi_0(r)(r^4 \beta^2 f F)$$

$$b_3 = \int_0^l \mathrm{d}r \, \psi_0(r)(r^4 \beta f F)\left[2\left(\frac{1}{r} + \frac{f'}{f}\right)\left(\frac{1}{r} + \frac{F'}{F}\right) + \frac{\beta'}{\beta}\left(\frac{2}{r} + \frac{f'}{f} + \frac{F'}{F}\right) + \frac{12}{r^2}\right]$$

$$b_4 = \int_0^l \mathrm{d}r \, \psi_0(r)(r^4 f F q(r))\left[\left(\frac{1}{r} + \frac{f'}{f}\right)\left(\frac{1}{r} + \frac{F'}{F} + \frac{q'}{q}\right) + \frac{6}{r^2}\right]$$

$$b_5 = \int_0^l \mathrm{d}r \, \psi_0(r)(r^5 \beta' f F)$$

$$b_6 = \int_0^l \mathrm{d}r \, \psi_0(r)(r^5 \beta^2 f F)\left(F + \frac{1}{r} - \frac{F'}{F} - \frac{\beta'}{\beta}\right)$$

where

$$q(r) \equiv \frac{4}{r^2} + \frac{F}{r} + F' - 4\frac{F'}{rF} - \frac{F''}{F}$$